SPIE's International Symposium on Interferometry in Space – Waikoloa, Hawaii USA – vol. 4852 – August 2002

Dim star fringe stabilization demonstration using pathlength feed-forward on the SIM Test-Bed 3 (STB3).

Renaud Goullioud*, Oscar S. Alvarez-Salazar, Bijan Nemati
Jet Propulsion Laboratory, 4800 Oak Grove Dr, Pasadena, CA91109

ABSTRACT

Future space-based optical interferometers such as the Space Interferometer Mission require fringe stabilization to the level of nanometers in order to produce astrometric data at the micro-arc-second level. Even the best attitude control system available to date will not be able to stabilize the attitude of a several thousand pound spacecraft to a few milli-arc-seconds. Active pathlength control is usually implemented to compensate for attitude drift of the spacecraft. This issue has been addressed in previous experiments while tracking bright stars. In the case of dim stars, as the sensor bandwidth falls below one hertz, feedback control will not provide sufficient rejection. However, stabilization of the fringes from a dim-star down to the nanometer level can be done open loop using information from additional interferometers looking at bright guide stars.

The STB3 testbed developed at the Jet Propulsion Laboratory features three optical interferometers sharing a common baseline, dynamically representative to the SIM interferometer. An artificial star feeding the interferometers is installed on a separate optics bench. Voice coils are used to simulate the attitude motion of the spacecraft by moving the entire bench. Data measured on STB3 show that fringe motion of a dim star due to spacecraft attitude changes can be attenuated by 80 dB at 0.1Hz without feedback control, using only information from two guide stars. This paper describes the STB3 setup, the pathlength feed-forward architecture, implementation issues and data collected with the system.

Keywords: interferometry, SIM, optics, pseudo-star

1. INTRODUCTION

Several testbeds [1,2,3] have been developed at the Jet Propulsion Laboratory under the Interferometry Technology Program to address the requirements raised by the Space Interferometry Mission (SIM). In particular, the Micro-Precision Interferometer (also called SIM System Testbed I), with a single baseline mounted on a truss structure, addresses several performance requirements of the control system. [2] However, the pathlength feed-forward algorithm cannot be tested on a single baseline interferometer. [4] This led to the development of the SIM system testbed 3 (STB3), a full 3-baseline interferometer representative of SIM. The main goal of the testbed is to demonstrate dim-star angle and fringe tracking by feeding-forward the information from two "guide" interferometers.

The development of the STB3 testbed is occurring in two phases (called phase 1 and 2) to address the complexity of the problem in two steps. [1] Phase 1 addresses the control system complexity and the pathlength feed-forward on a rigid table whereas phase 2 will address the extra complexity due to the flexibility of the flight-like structure and the external metrology system. This paper will focus on results achieved with the phase 1 setup. Bronowicki et al. [5] describes initial dynamics testing of the Phase 2 structure.

Phase 1 is a simpler version of the STB3 phase 2 with the following differences:

- Test-article mounted on top of a rigid table (instead of the flight-like structure).
- Smaller baseline: 4 meters instead of 8 meters.
- Common interferometric baseline instead of separate baselines.
- Single external metrology beam monitoring changes in the baseline (instead of the 3-D external metrology system).
- No need for absolute metrology.
- Visible metrology at 633 nm instead of infrared 1319 nm.

This paper presents first a quick overview of the architecture of STB3. Then it focuses on the pathlength feed-forward theory and implementation. A series of issues that had to be solved in order to increase the performance of the system is listed. Finally, we discuss experimental results obtained with the three interferometers running in feed-back and feed-forward mode.

* Send correspondence to: M/S:171-113, Phone: 818 354 7908, renaud@jpl.nasa.gov

2. TESTBED OVERVIEW

The testbed consists of two separate systems isolated from the ground: the pseudo-star and the test-article. Figure 1 shows a picture of the testbed. The layout and the hardware are described in more details by Goullioud et al. [6]

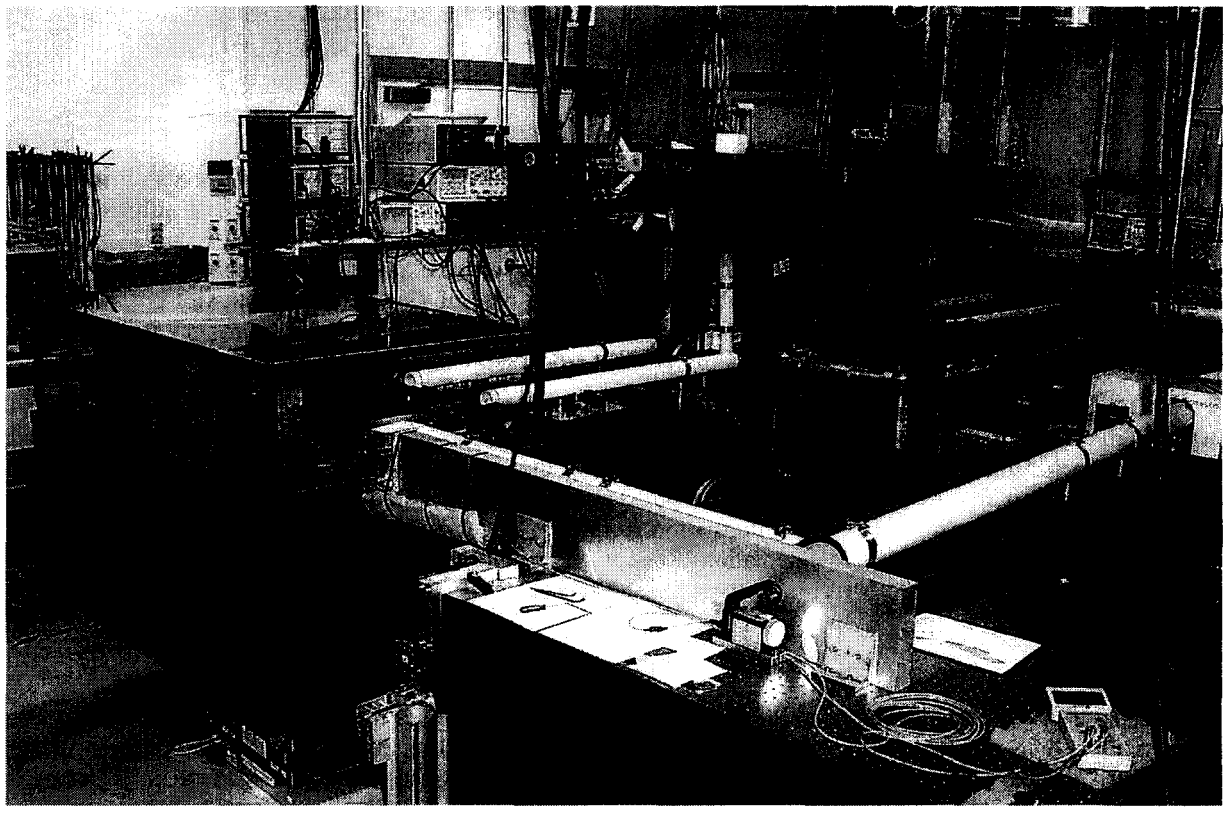

Figure 1: The STB-3 testbed. The pseudo-star table is nearest table. The test-article is on the second table, two beam combiner pallets are visible on top of the table (the first one is populated on both sides). The starlight paths are enclosed into pipe or plexiglass enclosures. The voice coils used for the ACS system are visible on the left side of the pseudo-star table

2. 1. Artificial star

The pseudo-star is a passive reverse interferometer mounted on a 5-meter long rigid table. A white light source coupled with a Nd:YAG laser produces the simulated stellar wavefront. A set of beam splitters and fold mirrors relay the pseudo-star wave front to each sides of the table. The originality of the design is the use of diffraction gratings to split the stellar wavefront into 3 stars. A stack of two transmission diffraction gratings divides the incoming beam into multiple beams with various configurations of diffraction order: zero-zero, zero-first, first-zero, first-first, zero-second, etc. The blazing of the grating lines disperses most of the light into the zero order and the first positive order. The undiffracted beam (zero-zero) is not deviated and is used for the "science" star. The zero-first order and first-zero order beams are used for the two "guide" stars. Sensitivity analysis has shown that common motion of the three stars is preferable to relative motion of one of the stars. The grating based configuration provides a relatively small sensitivity to mechanical vibration compared to a beam-splitter/mirror based design. [6] The three artificial stars are located at about 15 degrees from each other.

A metrology system (called "pseudo-star metrology") is used to monitor the behavior of the pseudo-star for diagnostic purpose and as an input sensor for rejection measurements described later in the article. It monitors only the external delay for the science baseline.

2. 2. Common baseline

The light coming from the pseudo-star travels through two spiders on each side of the test-article table. Corner-cubes, facing the test-article, are located at the center of each spider to retro-reflect the internal metrology beams. In fact, all three internal metrology beams share the same corner-cube on the TA side of the spider. The line going from the vertex of one corner-cube to the other corner-cube, 4.5 meters away, defines the common baseline of the system. The pseudo-star metrology reflects on the back side of the spiders, on smaller corner-cubes facing the pseudo-star side.

2. 3. Test-article

The Test-Article instrument is a triple Michelson interferometer mounted on top of a rigid 5-meter long honeycomb table. It is composed of two collector plates (East and West) and three beam combiner assemblies. Figure 1 shows the test-article with the combiner pallets on top. One interferometer is defined as the "Science" baseline whereas the two other ones are called "Guide" baselines. Each interferometer runs a CCD camera and two fast steering mirrors for angle tracking, and an avalanche photo-diode and an active optical delay-line for fringe tracking. An internal heterodyne laser metrology monitors the instrument optical path and controls the delay line position. Figure 2 and Figure 3 show the science beam combiner layout.

2. 4. Pathlength control

The electronics and the real-time control system are inherited from the RICST testbed. [7] The standard VME and VxWorks combination, with PowerPC processors is used. McKenney et al. [8] present in details the implementation of the various controllers in the real-time system.

The main actuator for pathlength control is the delay line (visible on the bottom of Figure 2). They are used to equalize the optical path between the two incoming starlight beams. The beam entering the delay line is focused on a flat secondary mirror by a parabolic mirror. The beam then leaves the delay line after reflecting back to the parabola mirror from the flat mirror. Only one of the two delay lines (the "active" delay line) is controlled.

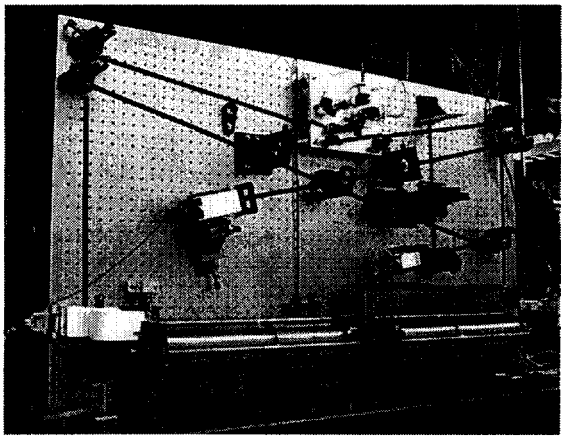

Figure 2: "Science" beam combiner. The two delay lines are visible on the bottom, the active one is on the left side of the picture. The metrology beam launcher plate is visible on the top. The metrology beams are injected into the starlight beams through holes at the center of folding mirrors.

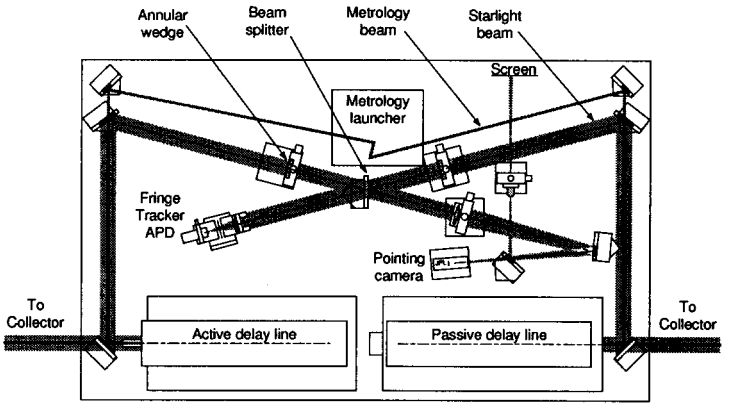

Figure 3: Beam combiner layout: Light coming from the collector enters first two delay lines, reflects onto a couple of folding mirrors and then reaches the beam splitter used to recombine the light. Two annular wedges are placed in each starlight beams before the beam splitter. The outer part of the beam, deviated by the wedges, will form two spots on the pointing camera when focused. The inner part of the beam, not affected by the wedges, is used for fringe tracking with the Avalanche Photodiode (APD).

There are three stages of controlling the optical pathlength in the active delay line: stepper motor, voice coil and two PZT stages. The stepper motor translates the whole delay line, while the voice coil only translates the optical tube on its flexures. The PZT stack translates the secondary mirror. The first PZT is used for pathlength control while the other PZT is modulated by a 1 kHz sawtooth wave in order to dither the fringe. The internal metrology is used to servo the three stages of the delay line at 5 kHz.

The recombined starlight beam is focused into a multimode fiber connected to an avalanche photodiode. A counter stores the photon counts in four even bins (binning at 5 kHz). The phase of the fringe is calculated every millisecond using the value of the four bins. Dithered fringe tracking is achieved by comparing the phase of the fringes with the phase of the 1 kHz sawtooth modulation. The phase error signal is then sent to the delay line servo.

3. PATHLENGTH FEED-FORWARD

SIM's science targets may be as dim as 20th magnitude stars, meaning they can be so dim that neither the pointing nor the pathlength control necessary for observing fringes can be performed using the signal from the science targets being observed. As a result, it is necessary to feed-forward the required pathlength and pointing control signals using internal and external metrology sensors as well as the guide interferometer measurements of the instrument attitude. The STB-3 testbed will attempt to demonstrate both technologies and has currently been solving the pathlength problem.

3. 1. Requirements

The goal of this experiment is to demonstrate stabilization of the fringes in the Science interferometer (Dim-Star mode) using the pathlength feed-forward of the fringe motion in the Guide interferometers (looking at Bright Stars). The effort has been focused in three objectives:

- Show an ambient stabilization of the Dim-star fringes to tens of nanometers under ambient lab conditions.
- Show rejection of the Dim-star fringe motion under SIM-like attitude motion down to the ambient noise in the lab.
- Measure rejection of the Dim-star fringe motion by 50 dB below 1Hz and 80dB below 0.1Hz.

NASA Headquarters had set a milestone for the STB3 team, as a part of the key-milestones for the technology program to demonstrate the feasibility of the Space Interferometry Mission. The objective was to demonstrate 50 dB of PFF rejection below 1Hz by December 2001.

3. 2. Theory

The basic elements of a stellar interferometer are shown in Figure 4. Light from a distant source is collected at two points and combined using a beam splitter, where interference of the combined wavefronts produces fringes when the internal pathlength difference (or delay) compensates exactly for the external delay. Thus, the angle between the interferometer baseline and the star can be found using the measured internal optical path difference (OPD), according to the relation:

$$\cos\alpha = \frac{\vec{B}\cdot\hat{s}}{B} = \frac{x}{B} \tag{3.1}$$

where x is the relative delay (OPD) of the wavefront to one side of the interferometer due to the angle. Thus, the astrometric angle α between the interferometer baseline and the ray from the star can be measured if the length of the baseline B and the internal delay are measured. In a stellar interferometer, the external metrology system measures the distance between two fiducials (each made of common-vertex corner cubes) and the internal metrology measures the optical path difference to the beam combiner from the two fiducials. Finally the starlight fringe detector measures the total optical path difference all the way to the star.

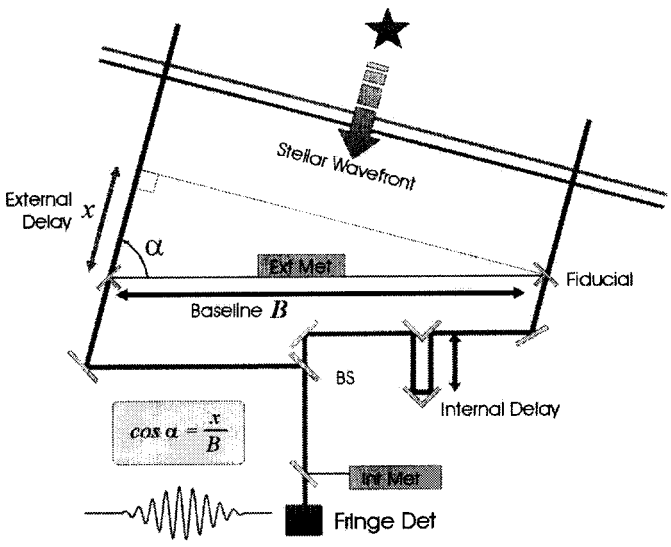

Figure 4: Basic stellar interferometer. The starlight fringe contrast is maximum when the internal delay matches the external delay, and is related to the baseline by the cosine of the astrometric angle

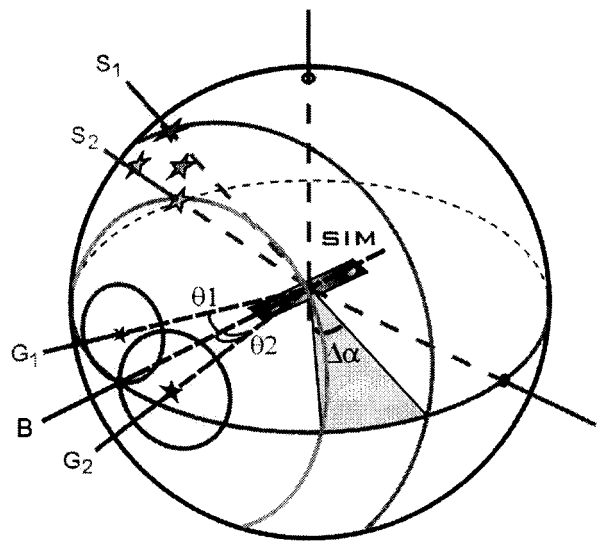

Figure 5: SIM astrometry requires two interferometers to track the science baseline vector with respect to designated "guide" stars, while a third interferometer measures projected angles among "science" targets.

SIM simultaneously employs three stellar interferometers to perform astrometry. Precision astrometry requires knowledge of the baseline orientation to the same order of precision as the astrometric measurement. To achieve this, a minimum of three interferometers is required. Two acquire and lock on bright "guide" stars, keeping track of the uncontrolled rigid-body motions of the instrument, while a third interferometer switches between science targets, measuring projected*

* When an interferometer measures an angle θ to a star, the stellar angular position is determined only to within a cone of half-angle θ with respect to the interferometer baseline. This is called a projected angle to highlight the fact that the difference of the measured angles to two different stars is in general different from the angle between the stars.

angles between them. These are shown in Figure 5. When the Guide 1 interferometer locks onto its target, G1, and measures an angle θ1 the orientation of the baseline B becomes constrained to pass through the circle** around G1. Similarly, locking on G2 and measuring an angle constrains the baseline to pass through the circle. With two guide interferometers locked and keeping track of the respective angles, the orientation of the baseline becomes limited to one of only two possibilities. From a-priori information the correct one can be chosen. Meanwhile the science interferometer measures the difference between the projected angles of pairs of science stars (S1, S2,...) in the region of interest. The final result is obtained by linking the results from the three interferometers and the external metrology system.

It should be noted that the precision metrology systems used on SIM measure length changes only. Thus, for example, when the Guide 1 interferometer locks on its target, it is only keeping track of the changes in the angle between the star and the baseline: the overall delay and hence the overall angle is not measured. Similarly, it is not the baseline vector that is measured by the external metrology system, but the changes in the baseline vector. The SIM approach is to perform a fit to the data after a large enough group of stars have been measured without losing fringe lock on the guide stars, and solve for these quantities later.

The primary goal in pathlength feed-forward (PFF) is to predict the observed science fringe position and compensate for its movements so that the fringes being formed on the science detector are stable during the relatively long integration times. The mathematical form for the PFF signal can be derived starting with the basic expression for the angle measured by an interferometer. Here, we derive the simpler common-baseline version of the feed-forward calculation applicable for the current phase of STB-3. The starting point is the basic astrometry formula (3.1) where $\vec{B}$ is the baseline vector with magnitude B, $\hat{s}$ is the unit vector to the star, and x is the internal OPD required to match the external delay. A change in the delay x can come from two sources:

$$\delta x = \delta\vec{B} \cdot \hat{s} + \vec{B} \cdot \delta\hat{s} \tag{3.2}$$

where the first term involves changes in the baseline vector, while the second term involves changes in the unit vector to the star. Since the star does not move, the second term is zero for SIM. Thus, in the PFF version of this equation, the $\delta\hat{s}$ term is explicitly dropped to produce a result applicable to SIM. This may seem invalid since in the lab, i.e. STB-3, the pseudo-stars do move. Nevertheless, since the PFF technique cannot rely on such external information, the term is dropped with the recognition that, in the presence of ambient instabilities, this stationary-star assumption may cause an error.

Focusing on the first term, the expression*** for the change in the baseline in terms of the changes in the magnitude and direction is:

$$\delta\vec{B} \approx B \cdot \delta\hat{b} + \delta B \cdot \hat{b} \quad \text{with} \quad \hat{b} \equiv \left(\vec{B} / B\right) \tag{3.3}$$

The first term is due to changes in the baseline orientation, e.g. errors arising from the attitude control system (ACS) dead-band. The second term captures the effect due to changes in the baseline length. Note that $\hat{b}$ is a unit vector and that the notation $\delta\hat{b}$ implies a change in the unit vector. We can now rewrite the delay change equation in terms of these variables:

$$\delta x = \delta B(\hat{b} \cdot \hat{s}) + B(\delta\hat{b} \cdot \hat{s}) \tag{3.4}$$

The expression for the PFF signal will look like the above equation, but will in the end be in terms of experimentally observable parameters. The quantity we need to stabilize is the science fringe position $\delta\phi_s$, which is equal to the sum of the external and internal delays:

$$\delta\phi_s = \delta x_s + \delta m_s \tag{3.5}$$

δm_s is simply the science internal metrology reading accounting for changes in the internal OPD of the science interferometer. It is the δx_s term that the feed-forward signal must provide, using equation 3.4:

$$\delta x_s^{FF} = \delta B(\hat{b} \cdot \hat{s}) + B(\delta\hat{b} \cdot \hat{s}) \tag{3.6}$$

In equation 3.6, the stellar direction to science star $\hat{s}$ is considered a known constant*. The variables $\hat{b}$ and B are also known to some a priori level. The baseline length change δB is measured with the external metrology system if needed. The

** Here, we assume a common-baseline configuration for the three interferometers, while SIM design assumes separate baselines.

*** The exact form for the baseline vector change contains a higher order cross term, proportional to $\delta B \cdot \delta\hat{b}$, which has been neglected.

* The science star direction $\hat{s}$, perhaps surprisingly, is considered a known quantity. The point here is that an estimate of the science star location is necessary in order to stabilize the fringes. Once the fringes are stabilized, a more precise measurement of $\hat{s}$ is obtained.

only quantity that is not directly available is $\delta\hat{b}$, which reflects the change in the baseline unit vector, which amounts to a rotation. It is the guide interferometers that are supposed to give us $\delta\hat{b}$. First, we note that we can write the analog of equation 3.4 for each of the guide interferometers for the two guide stars delay changes δx_{g1} and δx_{g2}:

$$\delta x_{g1} = \delta B(\hat{b}\cdot\hat{g}_1) + B(\delta\hat{b}\cdot\hat{g}_1) \tag{3.7}$$

$$\delta x_{g2} = \delta B(\hat{b}\cdot\hat{g}_2) + B(\delta\hat{b}\cdot\hat{g}_2)$$

These are two equations with only $\delta\hat{b}$ unknown. A third equation comes from a constrain on $\delta\hat{b}$ and $\hat{b}$ so that the change in the unit vector $\hat{b}$ leaves its length unchanged. Nemati [4] describes how to solve for $\delta\hat{b}$ using the linearly independent vectors $\hat{g}_1, \hat{g}_2$ and $\hat{n} = \hat{g}_1 \times \hat{g}_2$, he also derives the full quadratic PFF equations.

A simplified linear approximation of these equations has been used for this experiment. We have since found that a simplified version of the full PFF equation is adequate for baseline orientation changes up to 20 microradians, where it has a maximum error of one nanometer. This approximation, which assumes that the second-order effect of the baseline length change δB is negligible, reduces the PFF equation to:

$$\delta x_s^{FF} = C_1\delta x_{g1} + C_z\delta x_{g2} \tag{3.8}$$

$$\text{with } C_1 = \frac{1}{|\hat{g}_1\times\hat{g}_2|^2}\left[\hat{g}_1\cdot\hat{s} - (\hat{g}_2\cdot\hat{s})(\hat{g}_1\cdot\hat{g}_2) - \frac{\hat{n}\cdot\hat{s}}{\hat{n}\cdot\hat{b}}\left[\hat{b}\cdot\hat{g}_1 - (\hat{b}\cdot\hat{g}_2)(\hat{g}_1\cdot\hat{g}_2)\right]\right] \tag{3.9}$$

$$\text{and } C_2 = \frac{1}{|\hat{g}_1\times\hat{g}_2|^2}\left[\hat{g}_2\cdot\hat{s} - (\hat{g}_1\cdot\hat{s})(\hat{g}_1\cdot\hat{g}_2) - \frac{\hat{n}\cdot\hat{s}}{\hat{n}\cdot\hat{b}}\left[\hat{b}\cdot\hat{g}_2 - (\hat{b}\cdot\hat{g}_1)(\hat{g}_1\cdot\hat{g}_2)\right]\right] \tag{3.10}$$

The equation 3.8 applies to the common-baseline** (phase 1) configuration of the STB-3 testbed.

3. 3. Control

Based on the geometry of our artificial stars, the two PFF coefficients are:

$$C_1 = 1.92367 \quad \text{and} \quad C_2 = -0.88852 \tag{3.11}$$

Test on the laboratory shows that for the rigid honeycomb table, the changes in the baseline length δB during the length of an experiment are insignificant. In fact, the external metrology signal is dominated by the atmospheric noise. Thus, from equations 3.5 applied to the guide baselines and equation 3.8 with the numeric values 3.11, the PFF signal in terms of the measured quantities is:

$$\delta\phi_s^{FF} = 1.92367(\delta m_{g1} - \delta\phi_{g1}) - 0.88852(\delta m_{g2} - \delta\phi_{g2}) + \delta m_s \tag{3.12}$$

Figure 6 summarizes the controller implemented on the testbed. The fringe phase and the metrology signals from the Guide interferometers are low pass filtered in order to reduce the amount of noise fed-forward. The PFF target is then generated using equation 3.12. A lead filter compensates for the overall lag of the controller (due to the low filters and the delay line reaction time). The PFF target is then sent to the delay line to physically change the internal pathlength in the science interferometer. The internal metrology senses the change in delay and feeds back any remaining jitter in the internal path. The implementation of the controller on the real-time system is described in details by McKenney et al. [8]

The avalanche photo-diode measures the fringe position in the science beam combiner. However, this information cannot be used for control (to simulate the dim star); it is only recorded for the error metrics.

4. LESSONS LEARNED

4. 1. Fringe tracking

Fringe tracking performance in the guide interferometers plays a crucial role in path feed-forward performance; hence, improving the performance of fringe tracking feedback loops was necessary. For example, if the variables in equation 3.12 are considered noisy estimates of the true variables, then, to a first order, feed forward cannot perform better than the feedback loops on the guides. This is also evident by inspection of fringe error in each baseline, which is well correlated

** A three-baseline extension incorporating the enhanced external metrology system of SIM has also been derived.

outside the fringe tracker's bandwidth in all baselines. The current feedback loop on the guide interferometer has a unity gain at 30 Hz and about 10nm of jitter over all frequencies (Figure 11). The rejection, 40dB at 1Hz, 80dB at 0.1Hz and 120dB at 0.01Hz, is not a limiting factor in path feed-forward.

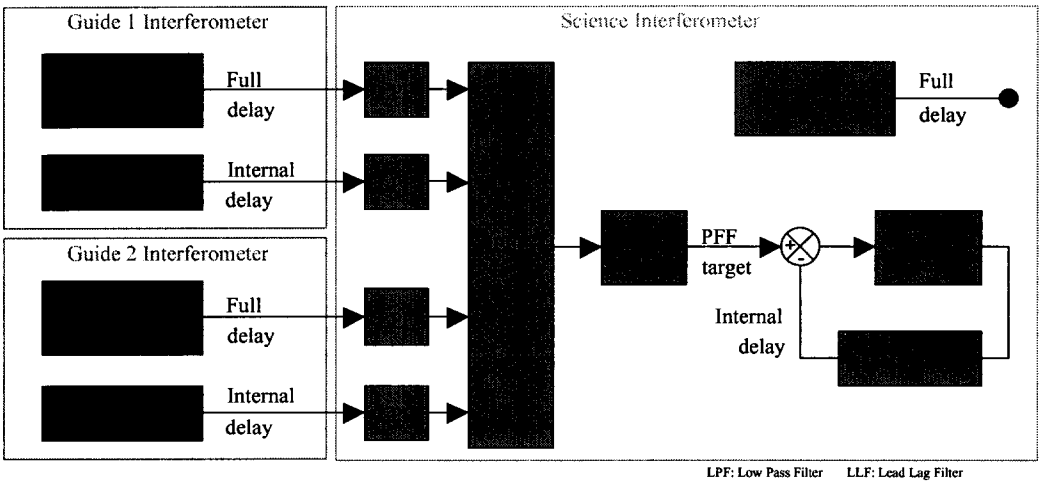

Figure 6: Pathlength Feed-Forward control implementation diagram

4. 2. High frequency noise filtering

If we assume the high frequency (above 100 Hz) noise in the signal coming from both guide interferometers to have equal mean and variance and to be uncorrelated (outside the band of the fringe trackers); then, using equation 3.12, the noise in the PFF signal is:

$$noise_s^{FF} = (1.92367 \oplus 0.88852)\, noise_g = 2.12\, noise_g \tag{4.1}$$

Equation 4.1 shows that the feed-forward signal has more than twice the noise in each of the guides. If not filtered, this noise is forwarded to the science baseline in PFF mode. In addition, because the noise is larger than the noise in each of the guide interferometers, it can cause the phase unwrapping algorithm in the science interferometer to exceed its range, even when the guide interferometers don't. To alleviate this problem, a 100 Hz second order Butterworth filter was implemented on all signals used to generate the PFF signal (to maintain relative phase). The 100 Hz bandwidth was selected to reduce the amount of lag introduced.

4. 3. Sampling rate

Since we were filtering the PFF signal down to 100Hz, we initially implemented the PFF task at 100Hz. Figure 7 shows a time trace of the initial implementation. One can see the PFF value updated at 100Hz and the Science internal metrology, closely following the PFF signal. However, the delay line servo with it 300Hz bandwidth is faster that the PFF updated rate. For the delay line servo, the PFF command signal is a succession of impulses. These impulses can be a few hundreds of nanometers high, causing a lot of noise in the science path and unwrapping errors of the science phase estimator. Increasing the PFF update rate higher than the delay line servo while keeping the same low pass filtering solved the issue. Currently, the PFF task is running at the same 1 kHz rate that the fringe trackers on the guide interferometers.

4. 4. Timing

The science delay line is the actuator used to implement the PFF signal. The internal metrology is used to control the delay line in feed-back. Comparing the Pseudo-Star metrology and the Science internal metrology gives us an indication of the delay of the feed-forward process, from the disturbance (change in the external delay), through filtering, to the correction (change in the internal delay). Figure 8 shows about 4 to 5 millisecond of delay between the external and the internal path length change. The timing delay will act as a phase delay for a periodic disturbance.

Assuming that the external pathlength change δx_s follows a sine wave of amplitude A and frequency f, and the internal pathlength change δm_s has a timing delay dt, the expression of the pathlength changes over time t is:

$$\delta x_s = A\sin[2\pi.f.t] \quad \text{and} \quad \delta m_s = -A\sin[2\pi.f.(t-dt)] \tag{4.2}$$

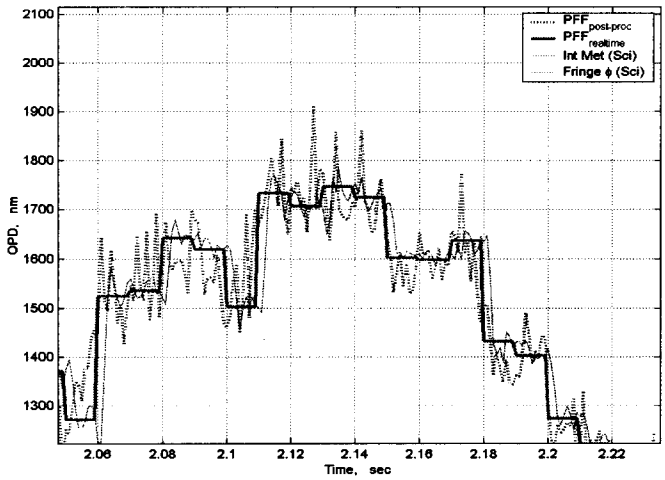

Figure 7: Time capture of the PFF signal in its initial 100Hz implementation.

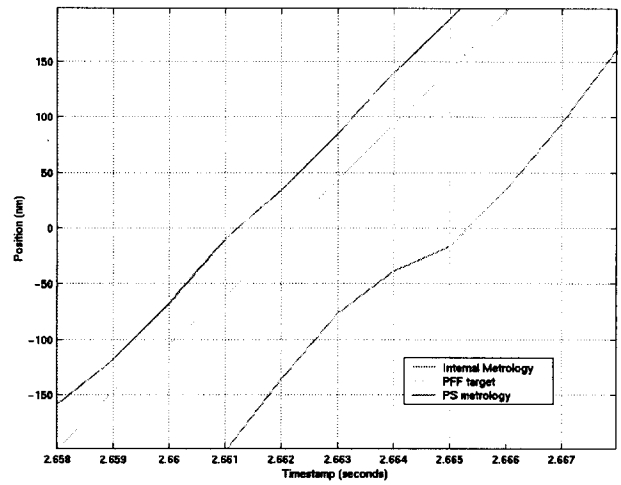

Figure 8: Zoom in the time capture of the PFF signal and internal metrology that shows 4ms of time delay

Using equation 3.5, we can calculate the motion of the fringes (overall pathlength error) for the science interferometer:

$$\delta\phi_s = A\sin[2\pi.f.t] - A\sin[2\pi.f.(t-dt)] \approx A'\sin[2\pi.f.t + \tfrac{\pi}{2}] \quad \text{with} \quad A' = 2A\sin[\pi.f.dt] \tag{4.3}$$

The timing delay dt produces a residual wave of amplitude A', reducing the rejection according to equation 5.1:

$$R_{(dB)} = 20\log\frac{\delta\phi_s}{\delta x_s} \approx 20\log\frac{A'}{A} \approx 20\log[2\sin(\pi.f.dt)] \tag{4.4}$$

If the timing delay dt is 5 ms, at 1Hz, the rejection is limited to -30dB and at 0.1Hz, the rejection is limited to -50dB. An empirical survey of the system showed no dependence of time delay on the frequency variable. Hence, to mitigate the delay, a lead-lag filter was implemented on the PFF signal to compensate for the total timing delay to better than 0.5ms at frequencies below 10 Hz.

4. 5. Phase unwrapping

We estimate the full optical path by comparing the fringe phase with the dither cycle. This process provides good accuracy, but does not provide the integer number of fringes. In fact, the real-time computer keeps track of the integer number of fringes as the phase wraps. However, there is an ambiguity if the phase suddenly jumps by half a wave: the unwrapper cannot solve for the integer part. The system usually recovers but the pathlength has changed by a full wave.

Figure 9 shows multiple occurrences of unwrapping errors: "Guide 1" trace suddenly jumps 500 nm (about one wave) at 8.87 s because of an unwrapping error. The delay line reacts quickly and brings the phase back to zero. However, the Guide 1 interferometer is now tracking the next fringe. Similarly, the Science trace jumps four waves at 9.2 s. Unwrapping errors are caused by electrical and mechanical noise. The solution was a combination of reduction of the electrical noise and damping of sharp mechanical modes. Furthermore, a low pass filter was put on the photon counts used by the phase unwrapper, which had the effect of reducing errors due to residual noise.

4. 6. Geometry

The PPF rejection is limited by the linearity and the knowledge (i.e., signal to noise ratio) of the parameters in Equation 3.12. In particular, the PFF coefficients C_1 and C_2 need to be known with a precision larger than the targeted PFF rejection above the noise floor. In the lab, the PFF coefficients were calculated based on the geometry of our artificial star, which yielded a resolution of about 10 arc minutes. After most other problems in the testbed were solved, the PFF rejection was limited to about 50dB at frequencies below 1 Hz. In order to show higher rejection, we needed to know the position of the pseudo-stars with higher resolution. Due to limitations in the lab, it was easier to run all three interferometer in feedback mode (as if we were looking at three bright stars) and solve for the geometry. This was done while rejecting a low frequency disturbance whose amplitude was at least 10^5 times greater than the PFF noise floor. The new PFF coefficients are now known to 10^{-5}, this corresponds to a resolution of 10 arc-seconds for the star positions.

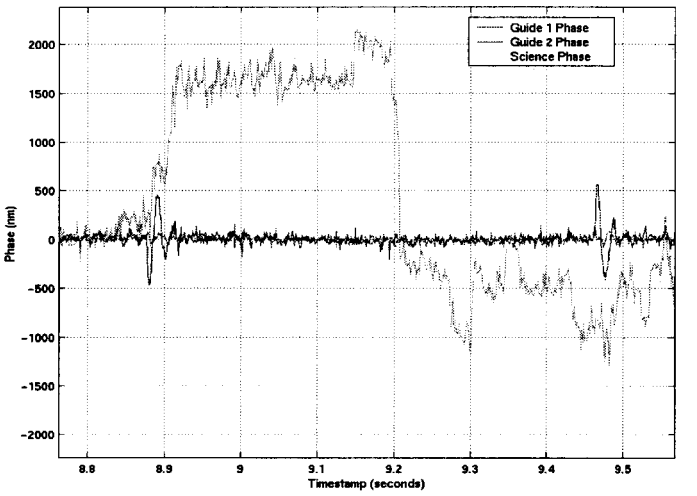

Figure 9: Phase unwrapping errors.

4. 7. Atmosphere

The use of common air paths in the pseudo star system removes the bulk of atmospherics-related error. On the other hand, the test article uses an internal metrology system on each interferometer to stabilize its internal path length difference, which include fluctuations due to the atmosphere. The problem with this system is that the starlight and metrology systems do not have common air paths; hence, some atmospheric fluctuations in the starlight propagation path are not stabilized. These fluctuations are then inevitably detected by the fringe tracking sensor (this is the error) in the guides, rejected as external optical delay, and subsequently used to generate the PFF signal.

All optical paths have been covered with either PVC pipes or Plexiglas enclosures (see Figure 1). Reducing the strength of atmospheric fluctuations in the test bed has mitigated the error due to these fluctuations (initially 200 nm of path-length error in the PFF signal, with the bulk of that happening below one Hertz). The atmosphere is still limiting our PFF noise floor but at a rate of only 30nm rms. Alvarez-Salazar et al. [9] performed a detail study of the atmospheric contribution with potential mitigation.

5. RESULTS

5. 1. Performance testing methodology

The goal of the test-bed is to demonstrate better than 10-nm fringe stability on the Science baseline while rejecting on-orbit like disturbances. However, the presence of atmospheric noise in the lab puts this goal out of reach in our current architecture. What is done instead of showing better than 10-nm fringe stability, is demonstrate the type of rejection levels expected of SIM. To do this, it is necessary to induce sufficiently large input disturbances and reject them down to the noise floor, which is invariant due to atmospherics. We use the Attitude Control System (ACS) to move the Pseudo-star table in all degreed of freedom. We have chosen to move the star rather than the instrument only because the center of mass was lower on the star table. The ACS system, described in details by Gursel et al. [10], is capable of moving the table up to a milliradian at frequency below 1Hz.

The purpose of the feed-forward loop is to stabilize the fringes, i.e. drive the path-length change to zero. Therefore, the error metric for assessing system feed-forward performance is simply the measured star fringe position $\delta\phi_s$ in the science beam combiner. The science star is supposed to be dim, however, the science pseudo star is made bright enough to allow fringe measurements for performance monitoring only (i.e., not used in any of the control loops).

5. 2. Ambient Performance

For the ambient test, the two guide interferometers are running the feed-back fringe tracker loops and the science interferometer is on PFF mode. In Figure 10, we show an 8 minute time capture. The pseudo-star metrology (PSM) monitors the ambient change in the external delay for the science baseline, about 1.5 μm rms. The Guide interferometers (G1 and G2) stabilized their path down to 20 nm with the feed-back loop. The science interferometer with the PFF control reduces the overall pathlength change from 1.5 μm down to 125 nm rms. Figure 11 shows the corresponding power spectra. One can see the high rejection of the feed-back loop on the Guide baselines, with the cross-over hump at 30 Hz. At 1.5 Hz, the resonance

of the table on the suspension system is obvious. From 0.001 Hz to 3 Hz, the PFF floor is visible on the "Science phase trace". This is the floor of our experiment, mostly limited by the atmosphere in the lab.

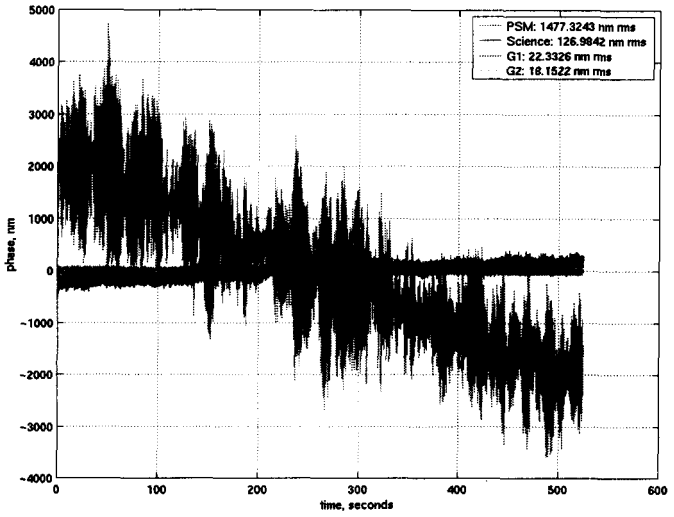

Figure 10: Ambient PFF performance, time capture

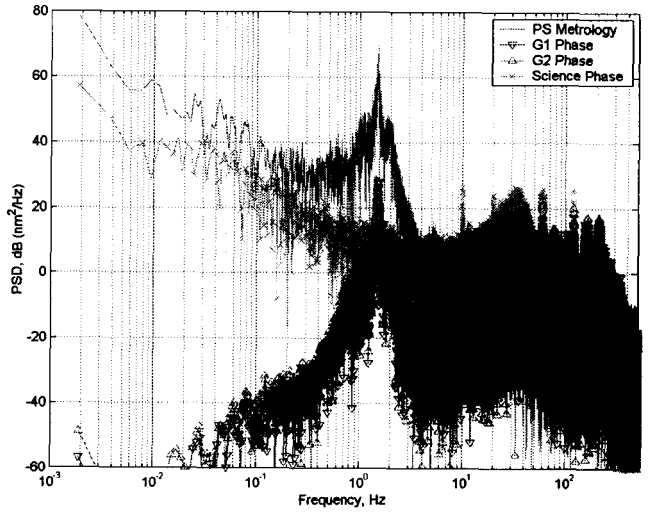

Figure 11: Ambient PFF performance, power spectrum

5. 3. Pathlength rejection

In order to quantify the performance of the PFF, we measure its ability to reject disturbances on the external path. We define the rejection in decibels:

$$R_{(dB)} = 20\log\frac{\delta\phi_s}{\delta x_s} \tag{5.1}$$

The rejection tests use the ACS system to inject a sinusoidal modulation of the external delay. For the test corresponding to Figure 12, the ACS actuates the table at 0.01Hz in the Yaw direction. This causes the external delay to vary by 75 microns rms. The 0.01Hz disturbance can be seen in the PSM trace. Comparing Figure 11 and Figure 12, one can observe that the Science Phase remains at the noise floor. The ACS disturbance is fully rejected (by about 80dB in that run).

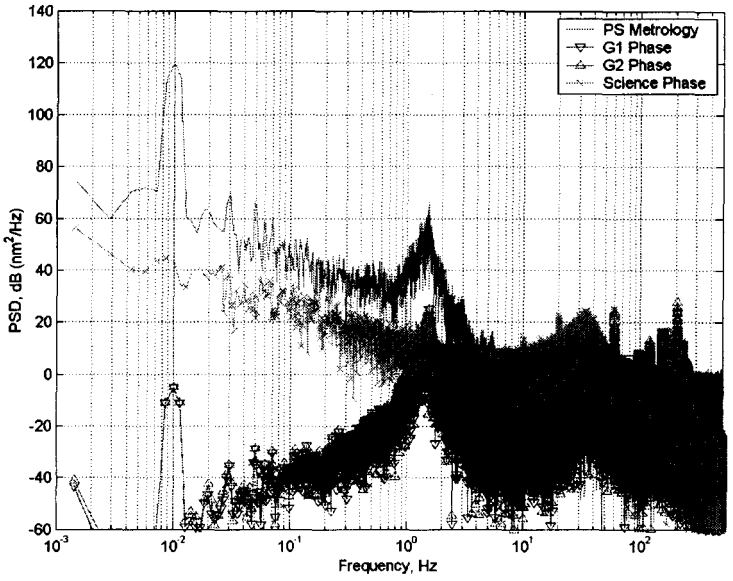

Figure 12: Pathlength Feed-Forward performance for an 0.01Hz sine attitude in the roll direction

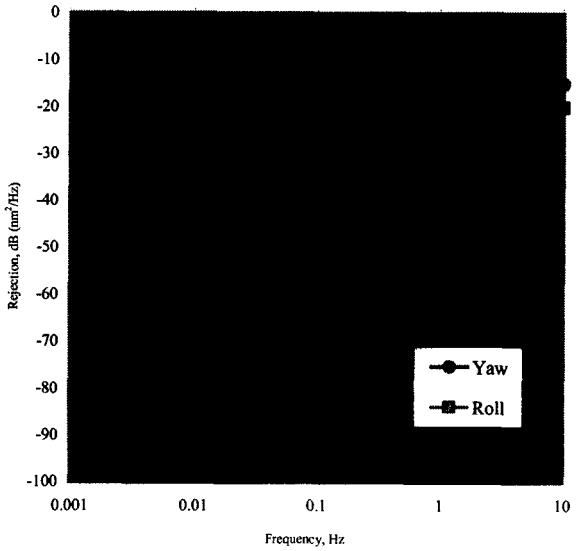

Figure 13: PFF Performance summary chart

Figure 13 summarizes the performance at multiple frequencies in the two degrees of freedom of interest. The rejection is increasing as the frequency is decreasing, up to 80dB. The 80dB rejection floor below 0.1Hz is a limitation of the testbed: the atmosphere limits the science phase $\delta\phi_s$ to a lower floor while the ACS system capability limits the pathlength modulation δx_s to an upper floor.

5. 4. On-orbit like results

For the third kind of test, we want to reproduce the on-orbit condition. Based on previously flown missions, it is possible to estimate the amount of attitude disturbance applied to the spacecraft from the solar winds, ACS error, etc. One such estimate was provided by TRW in the format of a power spectral density function. This function was realized in the testbed though a signal generation filter with a white gaussian noise input applied to the ACS system. Figure 14 shows the power spectrum density of the response of the pseudo-star table (PS metrology) to this on-orbit like disturbance. Figure 14 also the science phase while on PFF mode. Note how the on-orbit like disturbance is rejected, again, to the atmospheric noise floor. This floor will not be present in orbit, therefore, the performance is expected to be much better, below the 10nm allocation.

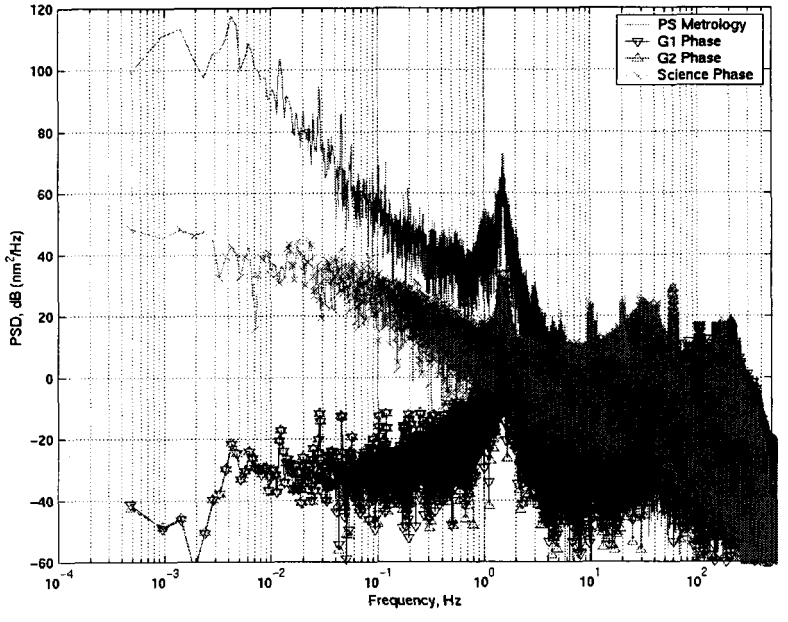

Figure 14: Performance for on-orbit like disturbance

5. 5. Combined feed-forward and feed-back

The previous tests do not make any use of the science star light for control. In practice, this will be only the case for the dimmest stars of magnitude 20 and higher. For a 15.5 magnitude science star, the integration time would be about one second. In the following series of tests, we combined the feed-forward command with a slow feed-back loop. For this so called "Dim-Star Fringe Tracking", the fringe phase information was sampled every seconds.

Figure 15 shows an ambient run of this mode. Comparing Figure 11 and Figure 15, one can see that below 0.04Hz, the feed-back loop rejects the PFF noise floor. The fringe motion in the science baseline is thus reduced to 30 nm rms from 0 to 1Hz. Figure 16 compares the pathlength rejection for the pathlength feed-forward only (PFF) and for the dim-star fringe tracking only (DSFT) with the combined control scheme. The data confirm that the two loops can be blended providing the cumulative rejection.

6. CONCLUSION

In this paper, we have presented the pathlength feed-forward control implemented on the SIM system testbed 3 to reject the optical pathlength variation on the science interferometer staring at a dim star. A sample of the issues encountered in the implementation of the controller has been listed. Experimental tests in the lab confirm the theory relative to the use of guide interferometers to control the pathlength of a third interferometer. Specifically, the data shows that this approach is sufficient to reject the on orbit disturbance and that rejections of 80dB and higher can be achieved. The results are critical for the Technology Program in order to predict SIM performance.

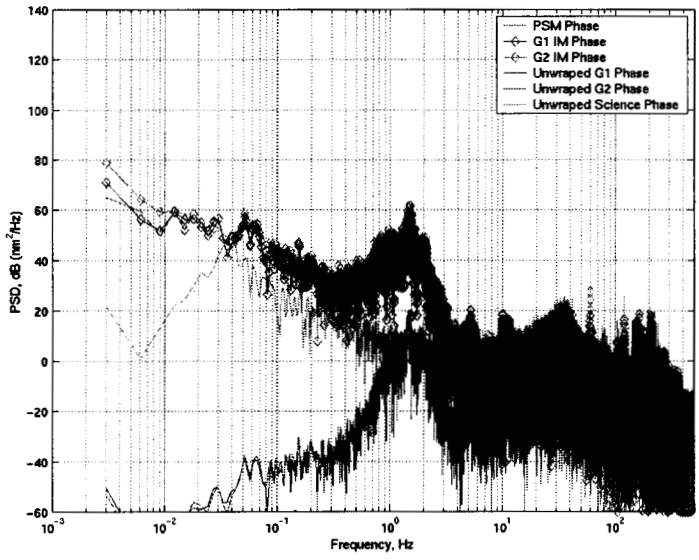

Figure 15: Combined Pathlength Feed-Forward and 1Hz-sample-rate Dim Star Fringe Tracking.

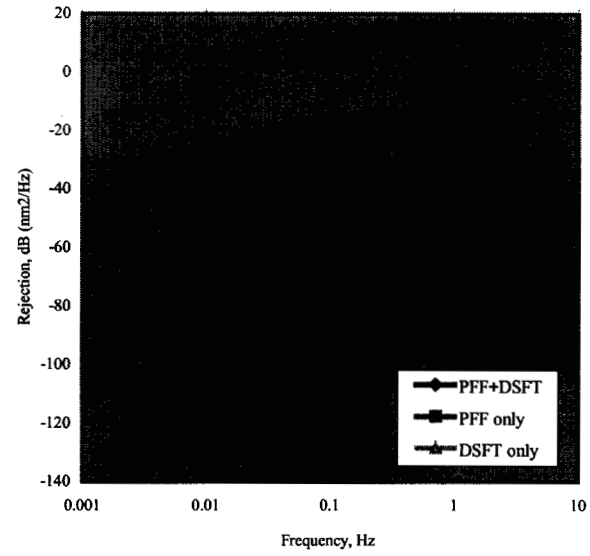

Figure 16: Summary chart: Pathlength Feed-Forward only, Dim Star Fringe Tracking only and combined performance.

ACKNOWLEDGEMENTS

The research described in this publication was performed at the Jet Propulsion Laboratory of the California Institute of Technology, under contract with the National Aeronautics and Space Administration. The results presented are the fruits of an entire team. The authors would like to thank in particular: Arshak Avanesyan, Alireza Azizi, Mike Deck, Jens Fischer, Rick Graves, Yekta Gursel, John Hench, Brad Hines, Phil Irwin, Elizabeth McKenney, Mario Mora, Martin Regehr, John Shaw, Robert Stephenson and George Sun.

BIBLIOGRAPHY

1. B. E. Hines, "SIM System Testbed III", *SPIE conference on Interferometry in Optical Astronomy*, vol. 4006, pp. 859-870, 2000.
2. R. Goullioud, F. G. Dekens and G. W. Neat, "Micro- Precision Interferometer: Scoreboard on technology Readiness for the Space Interferometer Mission", *SPIE conference on Interferometry in Optical Astronomy*, vol. 4006, pp. 847-858, 2000.
3. B. E. Hines, C. E. Bell, R. Goullioud, R. Spero, G. W. Neat, T. J. Shen, and E. E. Bloemhof, "Micro-arcsecond metrology (MAM) testbed overview," *SPIE conference Interferometry in Space*, vol. 4852, 2002.
4. B. Nemati, "Demonstration of pathlength feed-forward for precision dim-star astrometry", *SPIE conference on Interferometry in Optical Astronomy*, vol. 4006, pp. 905-914, 2000.
5. A. J. Bronowicki, R. MacDonald, Y. Gursel, R. Goullioud, T. Neville ,D. Platus, "Dual stage passive vibration isolation for optical interferometer missions," *SPIE conference Interferometry in Space*, vol. 4852, 2002.
6. R. Goullioud, A. Azizi, "Optical design of the SIM System Testbed 3", *SPIE conference on Interferometry in Optical Astronomy*, vol. 4006, pp. 788-799, 2000.
7. P. C. Irwin and R. Goullioud, "Hardware design and object-oriented hardware driver design for the Real-time Interferometer Control System Testbed", *SPIE Conference on Astronomical Interferometry*, vol. 3350, pp. 146-152, 1998.
8. E. A. McKenney, O.S. Alvarez Salazar, "SIM testbed 3 real-time control software," *SPIE conference Interferometry in Space*, vol. 4852, 2002.
9. O. S. Alvarez-Salazar, R. Goullioud, B. Nemati, A. Azizi, "Path feed forward performance of an astrometric 3-BL interferometer testbed (STB-3): mitigating atmospheric effects," *SPIE conference on Interferometry in Space*, vol. 4852, 2002.
10. Y. Gursel, E. A. McKenney, "Attitude control system for the SIM interferometry testbed 3 (STB-3)," *SPIE conference Interferometry in Space*, vol. 4852, 2002.